

Feature Engineering with Regularity Structures

August 13, 2021

I. Chevyrev¹, A. Gerasimovičs², and H. Weber³.

¹ The University of Edinburgh, Email: ichevyrev@gmail.com

² University of Bath, Email: ag2616@bath.ac.uk

³ University of Bath, Email: hw2025@bath.ac.uk

Abstract

We investigate the use of models from the theory of regularity structure as features in machine learning tasks. A model is a multi-linear function of a space-time signal designed to well-approximate solutions to partial differential equations (PDEs), even in low regularity regimes. Models can be seen as natural multi-dimensional generalisations of signatures of paths; our work therefore aims to extend the recent use of signatures in data science beyond the context of time-ordered data. We provide a flexible definition of a model feature vector associated to a space-time signal, along with two algorithms which illustrate ways in which these features can be combined with linear regression. We apply these algorithms in several numerical experiments designed to learn solutions to PDEs with a given forcing and boundary data. Our experiments include semi-linear parabolic and wave equations with forcing, and Burgers' equation with no forcing. We find an advantage in favour of our algorithms when compared to several alternative methods. Additionally, in the experiment with Burgers' equation, we noticed stability in the prediction power when noise is added to the observations.

Contents

1	Introduction	1
2	Models and regression algorithms	3
3	Numerical simulations	8
4	Summary and discussion	17
	Appendix A Motivation	18

1 Introduction

The aim of this paper is to explore the effectiveness of models from Hairer's theory of regularity structures [Hai14] as feature sets of space-time signals. A model is a collection of multi-linear functions of the signal which has been used to great success in the analysis of stochastic partial differential equations (SPDEs). This paper is the first, to our knowledge, to explore its effectiveness in a machine learning context.

One of the motivations for this study comes from the fact that models are a higher-dimensional analogue of the *path signature*, a central object in Lyons' theory of rough paths [Ly09]. The signature is the collection of the iterated integrals of a path,

which has a rich mathematical structure; it is known to characterise the path up to a natural equivalence relation [Che58, HL10, BGLY16] and leads to a natural notion of non-commutative moments on pathspace [CL16, CO18]. Over the past decade, the ability of the signature to encode information about a path in an efficient and robust way has made it a powerful tool in the analysis of *time-ordered data*. Examples of applications of signatures include the recognition of handwriting [XSJ⁺18, Gra13] and gestures [LZJ17], analysis of financial data [LNA19, KLA20], analysis of psychiatric and physiological data [AGG⁺18, MKN⁺19], topological data analysis [CNO20], neural networks [KBPA⁺19], and kernel learning [KO19, CO18].¹ See [CK16] for a gentle introduction to the path signature and some of its early applications.

We aim to partially address the natural question: can the signature be extended outside the context of time-ordered data, that is, to data parameterised by *multi-dimensional* space? To do this, we adapt the notion of a model from [Hai14] to define a *model feature vector* of a multi-dimensional signal (see Definition 2.3). The main difference between our definition and that in [Hai14] is that we suitably include the boundary data of the signal as part of the model. We point out that the path signature is a special case of our definition (see Example 2.8).

The basic problem on which we test the use of model feature vectors is:

Problem 1 *Given a space-time point (t, x) , predict the value $u(t, x)$, where u solves a PDE with unknown coefficients but with a known forcing ξ and initial condition u_0 .*

The idea to apply machine and statistical learning methods to find, predict, or study solutions of PDEs has seen much attention in recent years. See for example [MQdH18, RPK19, SS18, BSHHB19, HJE18, RBPK17] and the references therein. Many works in this direction have focused on new design of learning algorithms. In contrast, our main contribution comes from designing a new set of features which can be used in a range of algorithms. As such, we expect our approach to complement many existing methods. We describe in Appendix A the heuristic reason why models from regularity structures should serve as informative features for learning solutions to PDEs.

We propose two algorithms, Algorithms 1 and 2, in Section 2 based on elementary linear regression which use models as features in supervised learning tasks to address Problem 1. Algorithm 1 is designed to predict $u(t, x)$ in the presence of a general forcing ξ , while Algorithm 2 is designed to work when there is no forcing (or equivalently $\xi = 0$) in which case one can leverage the flow property of u to improve predictability. We investigate the effectiveness of these algorithms in numerical experiments in Section 3. We apply Algorithm 1 to non-linear parabolic and wave equations with forcing and fixed initial conditions, and apply Algorithm 2 to Burgers' equation with no forcing but varying initial condition.

In the case of Burgers' equation, Algorithm 2 dramatically outperforms an adaptation of the PDE-FIND algorithm [RBPK17] and a naive Euler scheme regression algorithm (see Section 3.3.1). Furthermore, in comparison to the other methods, our algorithm gives a reasonable prediction for Burgers' equation even when noise is added to the observed data. In the case of a parabolic equation, Algorithm 1 outperforms some basic off-the-shelf regression algorithms (SVM, K-Nearest Neighbours, Random forests) applied simply by treating the forcing as a large vector (see Remark 3.4).

Our algorithms come with several hyperparameters, one of which is the 'height' (number of iterated applications of a linear operator) of the model; in the case of path

¹[Gra13, MKN⁺19] notably received first prizes in the ICDAR 2013 competition and the PhysioNet 2019 Computing in Cardiology Challenge respectively.

signatures, our ‘height’ is the ‘level’ of a signature. In all the numerical experiments it was established that using a model with a larger height improves the performance of regression, up to a point when algorithms start to overfit. Another hyperparameter is the linear operator used in the definition of a model. In the case of Burgers’ equation we additionally found that the linear operator parameter can be ‘guessed’ from the data, yielding sensible results. Some further discussion is given in Section 4.

Finally, we emphasise that the methods presented in this paper extend, in principle, far beyond the scope of PDEs. The definition of the model in Section 2.1 and algorithms in Section 2 are presented independently of PDEs and could be applied to learn any output $u(t, x)$, not necessarily the solution of a PDE. Moreover, these algorithms can likely be adapted to settings where the output u does not depend explicitly on a point (t, x) , e.g., where u is a classification label used to classify the signal ξ . Such extensions, which are discussed further in Section 4, would parallel the current use of signatures in data science well beyond the scope of ODEs. We leave the systematic development of this theory to a future work.

Acknowledgments

AG and HW are supported by the Leverhulme Trust through a Philip Leverhulme Prize. HW is supported by the Royal Society through the University Research Fellowship UF140187.

2 Models and regression algorithms

In this section we introduce several algorithms based on models for learning functions of space-time signals.

2.1 Models

We denote by $\mathbb{N} = \{0, 1, 2, \dots\}$ the set of non-negative integers and by \mathbb{R} the set of real numbers. Assume that we are given a spatial domain $D \subset \mathbb{R}^d$ for $d \geq 0$ and a time horizon $T > 0$. The type of ‘signal’ we will consider is a function $\xi: [0, T] \times D \rightarrow \mathbb{R}$, which we call the *forcing*, and a family of functions $\{u^i\}_{i \in \mathcal{J}}$, $u^i: [0, T] \times D \rightarrow \mathbb{R}$, where \mathcal{J} is a finite index set. The case $d = 0$ corresponds to a just $\xi, u^i: [0, T] \rightarrow \mathbb{R}$. In the experiments in Section 3, we sometimes let u^i be fixed, so that the signal is only ξ , and sometimes we fix ξ (essentially taking $\xi \equiv 0$) so that the signal is only u^i .

Remark 2.1 For simplicity, the objects in this subsection are formulated in the continuum. In practice, however, one typically works with a finite approximation and would need to adjust the definitions accordingly; see, for instance, Sections 2.2 and 3 where we work on a grid.

Remark 2.2 At this stage, ξ and u^i look identical, but later on they will play different roles - while ξ is a space-time forcing, the u^i will be derived from an initial condition. See Example 2.4 for what u^i is in our experiments below.

Let us fix linear operator I that maps space-time functions $f: [0, T] \times D \rightarrow \mathbb{R}$ to some space-time functions $I[f]$. As an example $I[f]$ could be a convolution with some space-time kernel or a solution to some linear PDE with forcing f . Given a multi-index $a \in \mathbb{N}^d$, we denote by $\partial^a = \partial_1^{a_1} \dots \partial_d^{a_d}$ where

$$\partial_i^{a_i} := \frac{\partial^{a_i}}{\partial x_i^{a_i}}, \quad \text{for } i = 1, \dots, d.$$

We will also define the order of a multi-index as $|a| := \sum_{i=1}^d a_i$. Motivated by models from [Hai14, Sec. 8] we give the following definition.

Definition 2.3 Consider a tuple of non-negative integers $\alpha = (m, \ell, p, q) \in \mathbb{N}^4$ and $n \in \mathbb{N}$. Consider further a finite set \mathcal{J} (possibly empty), which we call *initialising symbols*. The *model feature set* \mathcal{S}_α^n is the finite set of formal symbols defined inductively by²

$$\begin{aligned} \mathcal{S}_\alpha^0 &= \mathcal{J}, \\ \mathcal{S}_\alpha^n &= \left\{ I[\xi^j \prod_{i=1}^k \partial^{a_i} \tau_i] : \tau_i \in \mathcal{S}_\alpha^{n-1}, a_i \in \mathbb{N}^d, |a_i| \leq q, j, k \in \mathbb{N}, \right. \\ &\quad \left. 0 \leq j \leq p, 1 \leq k+j \leq m\mathbf{1}_{j=0} + \ell\mathbf{1}_{j>0} \right\} \cup \mathcal{S}_\alpha^{n-1}. \end{aligned} \quad (2.1)$$

Consider a linear operator I . Assume we are given an input $(\{u^i\}_{i \in \mathcal{J}}, \xi)$ of functions $\xi, u^i: [0, T] \times D \rightarrow \mathbb{R}$. The *model feature vector* (or simply *model*) \mathcal{M}_α^n of (u^i, ξ) is the family (hash map) of functions

$$\mathcal{M}_\alpha^n = (f_\tau)_{\tau \in \mathcal{S}_\alpha^n}.$$

(As a hash map, \mathcal{M}_α^n has keys $\tau \in \mathcal{S}_\alpha^n$ and values f_τ .) The function $f_\tau: [0, T] \times D \rightarrow \mathbb{R}$ is defined recursively by $f_i = u^i$ for $i \in \mathcal{J}$ and for $\tau = I[\xi^j \prod_{i=1}^k \partial^{a_i} \tau_i]$

$$f_\tau = I[\xi^j \prod_{i=1}^k \partial^{a_i} f_{\tau_i}]. \quad (2.2)$$

We call n the *height* of a model, m the *additive width*, ℓ the *multiplicative width*, p the *forcing order*, and q the *differentiation order*. Furthermore,

- if $q = 0$, we call \mathcal{M}_α^n a *model without derivatives*,
- if $p = \ell = 0$, we call \mathcal{M}_α^n a *model without forcing*, and
- if \mathcal{J} is empty, we call \mathcal{M}_α^n a *model without initial conditions*.

Note that, on the right hand side of (2.2) ∂^{a_i} represents partial derivatives, I is an operator, and ξ is a function, while in the definition of τ all ∂^{a_i} , I and ξ are formal symbols. We will often use an abuse of notation and write $f_\tau \in \mathcal{M}_\alpha^n$ meaning that there exists a key $\tau \in \mathcal{S}_\alpha^n$ such that $\mathcal{M}_\alpha^n[\tau] = f_\tau$. The difference between additive and multiplicative width is the following: additive width m tells how many functions could be multiplied if they are not multiplied by the instance of the forcing ξ , while multiplicative width limits the total number of multiplications in the model.

Example 2.4 In all our experiments below, we will be given a set of ‘initial conditions’ $u_0^i: D \rightarrow \mathbb{R}$, $i \in \mathcal{J}$, and will derive $\{u^i\}_{i \in \mathcal{J}}$ from these initial conditions: in Section 3.3 \mathcal{J} will be a singleton $\mathcal{J} = \{c\}$ and $u^c = I_c[u_0](t, x)$ will be the solution to the heat equation with initial condition u_0 ; in Section 3.1 \mathcal{J} will primarily be empty $\mathcal{J} = \emptyset$; in Section 3.2 \mathcal{J} will contain two elements $\mathcal{J} = \{c, s\}$ which will correspond to the initial condition and speed respectively of the wave equation (see Definition 3.5).

²We use the convention $\prod_{i=1}^0 \tau_i = 1$. Furthermore, the product of symbols is commutative, e.g. we identify $I[\xi \partial^1 \tau_1 \partial^2 \tau_2] = I[\partial^2 \tau_2 \xi \partial^1 \tau_1]$, and multiplication by 1 is the identity, i.e. $1\tau = \tau$.

Remark 2.5 The symbols in \mathcal{S}_α^n can be represented as decorated combinatorial rooted trees as in [BHZ19, Sec. 2].

Remark 2.6 Definition 2.3 provides a middle ground between generality and readability. To make it more general, or adapt it to other situations, one could, for instance,

- include a forcing $\xi = \{\xi^i\}_{i=1}^K$ taking values in a multi-dimensional \mathbb{R}^K space by listing through all the components at each step in (2.1),
- include more than one operator or change operators for each height of the model,
- work with just a spatial domain $D \subset \mathbb{R}^d$, if there is no time direction present. In this case the linear operator I could be represented, for instance, by a kernel $K: D \times D \rightarrow \mathbb{R}$ with corresponding operator $I[f](x) = \int_D K(x, y)f(y) dy$.

Example 2.7 Consider $n = 1$, and $\alpha = (2, 2, 1, 1)$, and $d = 1$. Suppose $\mathcal{J} = \{c\}$ is a singleton. Then

$$\mathcal{S}_\alpha^1 = \{c, I[\xi], I[c], I[(c)^2], I[\xi c], I[\partial_x c], I[c \partial_x c], I[(\partial_x c)^2], I[\xi \partial_x c]\},$$

and if we take $\bar{\alpha} = (2, 2, 1, 0)$ i.e consider model without derivatives then

$$\mathcal{S}_{\bar{\alpha}}^1 = \{c, I[\xi], I[c], I[(c)^2], I[\xi c]\}.$$

Example 2.8 (Path signature) Consider the case $d = 0$, a multi-dimensional forcing $\xi = \{\xi^i\}_{i=1}^K: [0, T] \rightarrow \mathbb{R}^K$, and without initial conditions $\mathcal{J} = \emptyset$. Take $I[\xi](t) = \int_0^t \xi(s) ds$. By extending Definition 2.3 to multi-dimensional forcing as described in Remark 2.6, we recover precisely the level- n signature of the path $X(t) = \int_0^t \xi(s) ds$ from the model $\mathcal{M}_{(0,2,1,0)}^n$.

2.2 Regression algorithms

In this subsection, we propose two supervised learning algorithms which use the model feature vector of an input $(\{u^i\}_{i \in \mathcal{J}}, \xi)$ to learn an output u . While in principle there is no limitation of the nature of u (vector, classification label, etc.), we will consider the special case where u is a number associated to a space-time point or is a space-time function. In the experiments in Section 3, u will be the solution to a PDE with forcing ξ and a given initial condition.

To approximate the continuum, we fix a finite grid $\mathcal{O} \subset [0, T] \times D$ called the *observed points*. We will assume that $\mathcal{O} = \mathcal{O}_T \times \mathcal{O}_X$ where $\mathcal{O}_T = \{0 = t_0 < t_1 < \dots < t_N = T\}$ for some integer $N \geq 1$ and \mathcal{O}_X is a finite grid of points in D . As mentioned in Remark 2.1, we will work with functions defined on the grid \mathcal{O} instead of $[0, T] \times D$. For this purpose, both the operator I and the partial derivatives ∂_i must have an approximation on \mathcal{O} .

In the following algorithm, one should think of the observation u as a quantity which depends on the signal $(\{u^i\}_{i \in \mathcal{J}}, \xi)$ at a given space-time point $(t, x) \in \mathcal{O}$. Below $\{u^i\}_{i \in \mathcal{J}}$ and ξ will denote functions $u^i, \xi: \mathcal{O} \rightarrow \mathbb{R}$ for every $i \in \mathcal{J}$.

Algorithm 1 (Prediction at one point.)

Parameters: integers $n, m, \ell, p, q \in \mathbb{N}$ and an operator I .

Input:

- a point $(t, x) \in \mathcal{O}$;

- a set of initialising symbols \mathcal{J} ;
 - set of observed triplets $(u, \{u^i\}_{i \in \mathcal{J}}, \xi) \in U^{\text{obs}}$ where $u \in \mathbb{R}$;
 - a set of pairs $(\{u^i\}_{i \in \mathcal{J}}, \xi) \in U^{\text{pr}}$ for which we want to make a prediction.
- Output:** Prediction $u^{\text{pr}} \in \mathbb{R}$ for every $(\{u^i\}_{i \in \mathcal{J}}, \xi) \in U^{\text{pr}}$.

Step 1 Let $\alpha = (m, \ell, p, q)$. For each $(u, \{u^i\}_{i \in \mathcal{J}}, \xi) \in U^{\text{obs}}$ and each $(\{u^i\}_{i \in \mathcal{J}}, \xi) \in U^{\text{pr}}$ construct a model $\mathcal{M}_\alpha^n = (f_\tau)_{\tau \in \mathcal{S}_\alpha^n}$ using $\{u^i\}_{i \in \mathcal{J}}$ and ξ .

Step 2 Fit a linear regression of u against $(f_\tau(t, x))_{\tau \in \mathcal{S}_\alpha^n}$ for each $(u, \{u^i\}_{i \in \mathcal{J}}, \xi) \in U^{\text{obs}}$.

Step 3 For each $(\{u^i\}_{i \in \mathcal{J}}, \xi) \in U^{\text{pr}}$, construct a prediction u^{pr} using the linear fit constructed from Step 2 and the associated model \mathcal{M}_α^n .

Remark 2.9 Note that in Algorithm 1, we regress against the functions in the model at one input space-time point (t, x) only (see Appendix A for the motivation behind this choice in the case of PDEs). In the case of path signatures (Example 2.8), this corresponds to using only the endpoint of the signature, which is common practice (see e.g. [AGG⁺18, KO19, CNO20]).

We will now focus on predicting functions u at all space-time points which have a given initial condition and no forcing. Algorithm 2 below is designed to work when u satisfies the *time-homogeneous flow property*: $u(t, x)$ should depend on $u(0, \cdot)$ in the same way as $u(t + h, x)$ depends on $u(h, \cdot)$.

Assume that the observed time points \mathcal{O}_T are equally distanced. Let $\delta = T/N$ and $t_k = \delta k$ be the k -th observed time point. Assume that we are given an additional linear map I_c which is an *initialising map*: given $u_0: \mathcal{O}_X \rightarrow \mathbb{R}$, $I_c[u_0]$ is another function $\{0, \delta\} \times \mathcal{O}_X \rightarrow \mathbb{R}$.

Let $\mathcal{M}_\alpha^n(u_{t_k})$ be the model without forcing ($p = \ell = 0$) constructed on $\{0, \delta\} \times \mathcal{O}_X$ with $\mathcal{J} = \{c\}$ and $u^c := I_c[u_{t_k}]$.

We briefly describe the algorithm in words. Suppose that we know or have a prediction for $u(t_k, x)$ for some $k \in \{0, \dots, N-1\}$ and all $x \in \mathcal{O}_X$. Under the flow property, it is natural to seek an approximation for $u(t_{k+1}, x)$ in the form

$$u(t_{k+1}, x) \approx a + \sum_{\tau \in \mathcal{S}_\alpha^n} b_\tau f_\tau(\delta, x), \quad (2.3)$$

for every observed $x \in \mathcal{O}_X$ where $f_\tau \in \mathcal{M}_\alpha^n(u_{t_k})$. The time homogenous flow property implies that a and b_τ are expected to only depend on the time step δ and not t_k (we allow though a, b_τ to be x -dependent). In the training phase, we therefore decompose each observation $u: \mathcal{O} \rightarrow \mathbb{R}$ into N ‘subobservations’ $u(t_k + \cdot, \cdot): \{0, \delta\} \times \mathcal{O}_X \rightarrow \mathbb{R}$, for $k = 0, \dots, N-1$, and learn the coefficients a, b_τ from these subobservations. The prediction phase then recursively applies the formula (2.3) to predict u from the ‘initial condition’ $u(0, x)$. In the following, we will sometimes write u_t for the function $u(t, \cdot): \mathcal{O}_X \rightarrow \mathbb{R}$.

Algorithm 2 (Prediction using flow property.)

Parameters: integers $n, m, q \in \mathbb{N}$, operator I , and initialising map I_c .

Input:

- a collection $\{u(t, x)\}_{(t, x) \in \mathcal{O}} \in U^{\text{obs}}$ of observed functions;
- a collection $u_0 \in U^{\text{pr}}$ of initial conditions $u_0: \mathcal{O}_X \rightarrow \mathbb{R}$ for which we want to make a prediction.

Output: A prediction $u^{\text{pr}} : \mathcal{O} \rightarrow \mathbb{R}$ for every $u_0 \in U^{\text{pr}}$.

- Step 1* Let $\alpha = (m, 0, 0, q)$. For $k = 0, \dots, N-1$ and each $u \in U^{\text{obs}}$ construct a model $\mathcal{M}_\alpha^n(u_{t_k})$ on $\{0, \delta\} \times \mathcal{O}_X$ with $\mathcal{J} = \{c\}$ and $u^c = I_c[u_{t_k}]$.
- Step 2* For each observed $x \in \mathcal{O}_X$ fit a linear regression of $(u(t_{j+1}, x))_{u \in U^{\text{obs}}, j=0, \dots, N-1}$ against $((f_\tau(\delta, x))_{f_\tau \in \mathcal{M}_\alpha^n(u_{t_j})})_{u \in U^{\text{obs}}, j=0, \dots, N-1}$.
- Step 3* For each $u_0 \in U^{\text{pr}}$ construct a model $\mathcal{M}_\alpha^n(u_0)$ on $\{0, \delta\} \times \mathcal{O}_X$ with $\mathcal{J} = \{c\}$ and $u^c = I_c[u_0]$. Make a prediction of $u^{\text{pr}}(t_1, x)$ for each observed $x \in \mathcal{O}_X$ based on the fit from Step 2 and $(f_\tau(\delta, x))_{f_\tau \in \mathcal{M}_\alpha^n(u_0)}$.
- Step 4* Recursive step. For each $u_0 \in U^{\text{pr}}$, $k \geq 1$ and the predicted $u_{t_k}^{\text{pr}}$ construct a model $\mathcal{M}_\alpha^n(u_{t_k}^{\text{pr}})$ on $\{0, \delta\} \times \mathcal{O}_X$ with $\mathcal{J} = \{c\}$ and $u^c = I_c[u_{t_k}^{\text{pr}}]$ and make a prediction of $u^{\text{pr}}(t_{k+1}, x)$ for each observed $x \in \mathcal{O}_X$ based on a linear fit from Step 2 and $(f_\tau(\delta, x))_{f_\tau \in \mathcal{M}_\alpha^n(u_{t_k}^{\text{pr}})}$.

When specific boundary values are given one might need to enforce these for the predicted function u^{pr} . For example one might set $u^{\text{pr}}(t_k, x) = 0$ for $x \in \partial D$ and every $k = 0, \dots, N$ if this was known.

As remarked earlier, Algorithm 2 effectively converts the size of the training set for the linear fit from $|U^{\text{obs}}|$ to $N \times |U^{\text{obs}}|$.

Remark 2.10 Algorithm 2 aims to address a problem similar to that of learning a dynamical system. A different approach to this problem is dynamic mode decomposition, which is based on spectral analysis of the Koopman operator [Sch10, RMB⁺09].

Remark 2.11 Since the model $\mathcal{M}_\alpha^n(u_{t_k})$ only depends on the data $u_{t_k} : \mathcal{O}_X \rightarrow \mathbb{R}$, one could use an arbitrarily fine grid of $[0, \delta]$ (instead of just the endpoints $\{0, \delta\}$ as above) in order to construct the functions $f_\tau \in \mathcal{M}_\alpha^n(u_{t_k})$ if the approximations of I_c and I allow, which could lead to a better estimate of $u(t_{k+1}, x)$ by $(f_\tau(\delta, x))_{f_\tau \in \mathcal{M}_\alpha^n(u_{t_k})}$.

Remark 2.12 The cardinality of \mathcal{S}_α^n grows exponentially with n . To avoid overfitting or to speed up the learning, it can be important to restrict further the number of elements in \mathcal{S}_α^n . We do this below by introducing a function called *degree*³ $\text{deg} : \mathcal{S}_\alpha^n \rightarrow \mathbb{R}$ which satisfies

$$\text{deg} I[\tau] = \beta + \text{deg} \tau, \quad \text{deg} \partial^{a_i} \tau = \text{deg} \tau - |a_i|, \quad \text{deg} \prod_{i=1}^k \partial^{a_i} \tau_i = \prod_{i=1}^k \text{deg} \partial^{a_i} \tau_i, \quad (2.4)$$

for some $\beta > 0$. This definition is set so that deg of symbols from \mathcal{S}_α^n will be usually larger for bigger n, m, ℓ, p, q . We will then perform the regression in our algorithms against the functions in the model whose symbol does not exceed a certain degree γ . When used, the degree function and cutoff γ are additional parameters in Algorithm 1.

It is generally advised to have the ratio (number of train cases):(number of predictors) above 10 (see [HJLC⁺84]). Thus, one would choose γ so that the number of functions in $f_\tau \in \mathcal{M}_\alpha^n$ with $\text{deg} \tau \leq \gamma$ is at least 10 times smaller than number of triplets in U^{obs} .

Note that it is much easier to keep the train cases to predictors ratio above 10 for Algorithm 2 because we have $N|U^{\text{obs}}|$ number of train cases compared to only

³The notion of degree is similar to the one introduced in [Hai14] and is related to the Hölder regularity of functions in the model which are built from highly oscillatory signals.

$|U^{\text{obs}}|$ train cases in Algorithm 1. Nevertheless, it is still beneficial to use degree for Algorithm 2 for computational reasons. Indeed, the linear regression time complexity for Algorithm 2 is $O(a^2(a+b))$, where $a = |\mathcal{M}_\alpha^n|$ and $b = N|U^{\text{obs}}|$. Thus, a large size of the model can drastically slow down the learning.

3 Numerical simulations

The principle example of a function of (u_0, ξ) that we wish to learn in this work is given by a solution to the following PDE on $[0, T] \times D$

$$\begin{aligned} \mathcal{L}u &= \mu(u, \partial_1 u, \dots, \partial_d u) + \sigma(u, \partial_1 u, \dots, \partial_d u)\xi, \\ u(0, x) &= u_0(x), \end{aligned} \quad (3.1)$$

where $u_0 : D \rightarrow \mathbb{R}$ is the initial condition⁴, \mathcal{L} is a linear differential operator whose inverse will be an operator I . The functions $\mu, \sigma : \mathbb{R} \times \mathbb{R}^d \rightarrow \mathbb{R}$ are assumed to be smooth. Such an equation is often called a *PDE with forcing* ξ . When ξ is a random function, e.g. space-time white noise, it is also referred to as a *stochastic* PDE (SPDE).

In general one needs to specify the boundary conditions of the above equation, i.e. the values of $u(t, x)$ for $x \in \partial D$. For simplicity, we only consider periodic boundary conditions in our experiment, but Dirichlet or Neumann boundary conditions can be easily implemented.

In all experiments below we use an ordinary least squares linear regression. See <https://github.com/andrisger/Feature-Engineering-with-Regularity-Structures.git> for Python code containing implementation of the model and experiments from this section.

3.1 Parabolic PDEs with forcing

In this subsection we will suppose that the differential operator in (3.1) is given by $\mathcal{L} = \partial_t - \nu \Delta$, where $\nu > 0$ is the viscosity and $\Delta = \sum_{i=1}^d \partial_i^2$ is the Laplacian on $D \subset \mathbb{R}^d$. This motivates the following definition.

Definition 3.1 Fix an initial condition $u_0 : D \rightarrow \mathbb{R}$ and a forcing $\xi : [0, T] \times D \rightarrow \mathbb{R}$ as well as $n, m, \ell \geq 1$. Let $p = 1$ and $q \leq 1$ so that $\alpha = (m, \ell, 1, q)$. The model for the parabolic equation \mathcal{M}_α^n is constructed by taking $\mathcal{J} = \{c\}$ with $u^c = I_c[u_0]$ where operators I and I_c are given by

$$\begin{cases} (\partial_t - \nu \Delta)I[f] = f, \\ I[f]_0 = 0, \end{cases} \quad \begin{cases} (\partial_t - \nu \Delta)I_c[g] = 0, \\ I_c[g]_0 = g, \end{cases} \quad (3.2)$$

for functions $f : [0, T] \times D \rightarrow \mathbb{R}$ and $g : D \rightarrow \mathbb{R}$, subject to the same boundary conditions as in (3.1).

The heuristic reason why Algorithm 1 should work for predicting PDEs comes from the fact that functions in \mathcal{M}_α^n constructed from $I_c[u_0]$ and ξ well approximate the n -th Picard iterate which itself should converge to the solution of (3.1) for smooth μ and σ . The reason to take $p = 1$ and $q \leq 1$ is respectively because the forcing ξ appears only once and because there could be at most one derivative on the right-hand side of (3.1). See more details in the Appendix A.

⁴One might need to include other initial information like an initial speed for the case of the wave equation from section 3.2.

Remark 3.2 Algorithm 1 does not require knowledge of μ or σ . However, in the experiments in this subsection, μ and σ will be polynomials, and we will use knowledge of their degree to choose the hyperparameters m, ℓ . Another hyperparameter is ν since this determines I through (3.2). When μ, σ, ν are completely unknown, these hyperparameters could be chosen, as usual, by splitting the data into training, validation and test sets, and tuning the hyperparameters on the validation set. See also Section 3.3 where a starting point for an approximation of the viscosity $\tilde{\nu}$ is derived from the training data.

3.1.1 Multiplicative forcing

Consider the following PDE

$$\begin{aligned} (\partial_t - \Delta)u &= 3u - u^3 + u\xi \quad \text{for } (t, x) \in [0, 1] \times [0, 1], \\ u(t, 0) &= u(t, 1) \quad (\text{Periodic BC}), \\ u(0, x) &= x(1 - x), \end{aligned} \tag{3.3}$$

where ξ is a space-time forcing. Here we discretise space and time respectively in 100 and 1000 evenly distanced points, which we use to define the grids \mathcal{O}_X and \mathcal{O}_T . We solve (3.3) for each forcing ξ using a finite difference method on the same discretisation $\mathcal{O} = \mathcal{O}_T \times \mathcal{O}_X$ (see [LPS14, Sec. 10.5]).

We take here ξ as approximations of space-time white noise. We perform Algorithm 1 both using the full model \mathcal{M}_α^n from Definition 3.1 and the model without the initial conditions (i.e. where \mathcal{J} is assumed to be empty in the construction of \mathcal{S}_α^n). We have found that in practice using the full model did not drastically improve the errors (see Remark 3.3). Therefore, we primarily present results in this subsection for the model without the initial condition.

We construct a model with $\mathcal{J} = \emptyset$ of height $n = 4$, additive width $m = 3$, multiplicative width $\ell = 2$ and take $q = 0$ (because μ and σ do not depend on ∂_i) so that $\alpha = (3, 2, 1, 0)$.⁵ We assign a degree from Remark 2.12 to satisfy (2.4) with $\beta = 2$ and $\deg \xi = -1.5$.⁶ In the experiments below we only consider functions $f_\tau \in \mathcal{M}_{3,1}^4$ with $\deg \tau \leq 5$.

We randomly sample 1000 realisations of approximations of white noise ξ on \mathcal{O} and solve (3.3) for each realisation. We then split the pairs (u, ξ) into training and test sets of size 700 and 300 respectively. There are only 56 functions in $f_\tau \in \mathcal{M}_\alpha^4$ with degree $\deg \tau \leq 5$ thus corresponding to a ratio of training cases to the number of predictors of $700/56 = 12.5$. In Figure 1, we show results of performing Algorithm 1 with models without initial conditions at various space-time points (t, x) . In every subfigure one can see a scatter plot of actual values of $u(t, x)$ from the test set plotted against the predicted values. The error is measured as a relative l^2 error and the slope of the regression line between true values and the predicted ones is included.

⁵See Remark A.1 for a motivation behind taking these particular widths.

⁶This is motivated by the Hölder regularity of space-time white noise being $-1.5 - \varepsilon$ for any small $\varepsilon > 0$ and the fact that the heat operator I increases the Hölder regularity by 2.

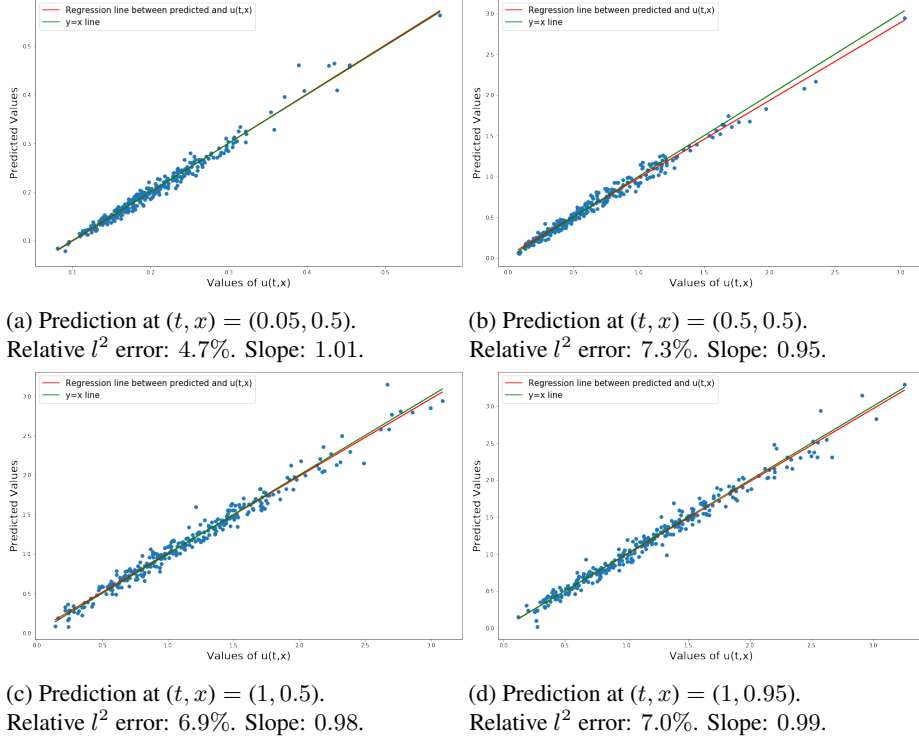


Figure 1: Results of linear regression of solution to (3.3) against the functions in model \mathcal{M}_α^4 with $\alpha = (3, 2, 1, 0)$, without initial conditions and of degree ≤ 5 . The x -axis contains values of $u(t, x)$ for realisations of the forcing ξ from the test set and the y -axis contains predictions of the linear regression. Subplots (a), (b), (c), (d) show predictions at space-time points $(t, x) = (0.05, 0.5), (0.5, 0.5), (1, 0.5), (1, 0.95)$ respectively.

In Figure 1 one sees a better fit for a small time $t = 0.05$ which is explained by the fact that the approximation of u by functions from \mathcal{M}_α^4 is local because of the Taylor expansions in the Picard iterations (see Appendix A). For larger times $t \in \{0.5, 1\}$ as well as different spatial points $x \in \{0.5, 1\}$ there seem to be no big statistical difference in accuracy.

	$(t, x) = (0.05, 0.5)$		$(t, x) = (0.5, 0.5)$		$(t, x) = (1, 0.5)$		$(t, x) = (1, 0.95)$	
Model's Height	Error	Slope	Error	Slope	Error	Slope	Error	Slope
1	8.83%	0.91	21.14%	0.85	22.81%	0.72	22.95%	0.75
2	5.60%	0.96	9.79%	0.97	13.42%	0.91	13.16%	0.91
3	5.15%	0.97	8.15%	0.98	7.90%	0.97	8.69%	0.96
4	4.88%	0.97	7.85%	0.98	6.61%	0.98	7.06%	0.98

Table 1: Relative l^2 errors and slopes for linear regression against models of different heights. Prediction is performed at space-time points $(t, x) = (0.05, 0.5), (0.5, 0.5), (1, 0.5), (1, 0.95)$.

In Table 1, we show relative l^2 errors and slopes of the regression line for Algorithm 1 applied to models of heights 1, 2, 3 and 4. All experiments are performed 1000 times (i.e. splitting the data randomly onto training/test sets) and the average values for error and slope over experiments is shown. Table 1 suggests that increasing height indeed allows for a better overall prediction. A similar result holds true for the width: additive width smaller than 3 (which corresponds to the third power in the non-linearity in (3.3)) gives on average a worse error.

Remark 3.3 Note that the error for the middle time $t = 0.5$ is slightly worse than for the end time $t = 1$. This could be caused by using a model without initial conditions instead of the full model. Indeed, using the full model as in Definition 3.1 allows to slightly reduce the error for the prediction at $(t, x) = (0.5, 0.5)$ to 7.4% (with the same $n = 4$ and $\alpha = (3, 2, 1, 0)$) while making almost no change to the error for the prediction at $(t, x) = (1, 0.5)$ and at $(t, x) = (0.05, 0.5)$.

The heuristic reason why the effect of the fixed initial condition could be ignored for the parabolic equations could be a good local structure and dissipative properties of the heat operator. The advantage of using models with $\mathcal{J} = \emptyset$ for parabolic equations is that such models contain fewer functions, which both improves the speed of the computation and might help with problems of overfitting.

Remark 3.4 We compare the results from Algorithm 1 with several basic off-the-shelf learning algorithms. To do this, for $(u, \xi) \in U^{\text{obs}}$ we transform all the space-time points of the forcing ξ into a vector (in this case a vector of 100000 points) and applied SVM, K-nearest neighbours, and Random Forest regressions to predict the value of $u(t, x)$ for some observed and fixed $(t, x) \in [0, T] \times D$. None of these algorithms gave better than 30% error at $(t, x) = (1, 0.5)$. Moreover, neither scaling the data, nor taking less space-time points of ξ , nor increasing the number of functions in U^{obs} drastically improved the error.

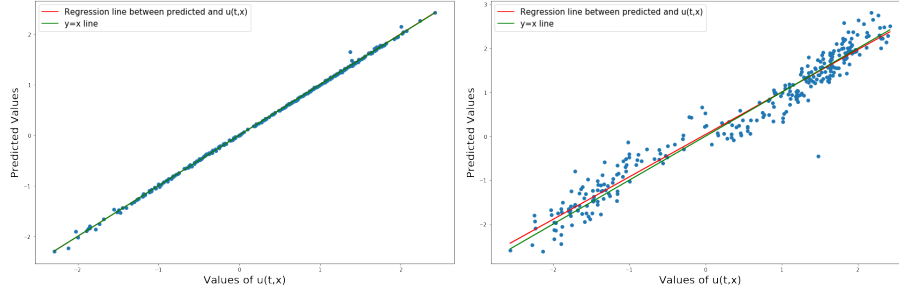
3.1.2 Additive forcing

We repeat the same experiment for the additive version of the equation (3.3) namely:

$$\begin{aligned} (\partial_t - \Delta)u &= 3u - u^3 + \xi \quad \text{for } (t, x) \in [0, 1] \times [0, 1], \\ u(t, 0) &= u(t, 1) \quad (\text{Periodic BC}), \\ u(0, x) &= x(1 - x). \end{aligned} \tag{3.4}$$

Discretisation of space-time and number of training and test cases is the same as in Section 3.1.1. For this we use model \mathcal{M}_α^5 with $\alpha = (3, 1, 1, 0)$, without initial conditions ($\mathcal{J} = \emptyset$), degree ≤ 7.5 , and Algorithm 1 which gives 58 functions.⁷ Note that since multiplicative width is 1 this reduces number of functions in the model, which allows us to take a larger height and upper bound for the degree. Figure 2 shows the results for space-time points $(t, x) = (0.5, 0.5)$ and $(t, x) = (1, 0.5)$. One can see that the additive equation exhibits a worse prediction for long times but a slightly better prediction for short times (for $t = 0.05$ error is even better: 0.1% in comparison to $\approx 5\%$ in the multiplicative case).

⁷See Remark A.1 for a motivations behind taking these particular widths.



(a) Prediction at $(t, x) = (0.5, 0.5)$.
Relative l^2 error: 5.9%. Slope: 1.01.

(b) Prediction at $(t, x) = (1, 0.5)$.
Relative l^2 error: 19.8%. Slope: 0.96.

Figure 2: Results of linear regression of solution to (3.4) against the functions in model \mathcal{M}_α^5 with $\alpha = (3, 1, 1, 0)$, without initial conditions and of degree ≤ 7.5 . The x -axis contains values of $u(t, x)$ for realisations of the forcing ξ from the test set and the y -axis contains predictions of the linear regression. Subplots (a), (b) show predictions at space-time points $(t, x) = (0.5, 0.5)$ and $(t, x) = (1, 0.5)$ respectively.

3.2 Wave equation with forcing

We will now consider a wave equation taking $\mathcal{L} = \partial_t^2 - \Delta$ in (3.1) and predict solutions of the following non-linear wave equation

$$\begin{aligned}
 (\partial_t^2 - \Delta)u &= \cos(\pi u) + u^2 + u\xi \quad \text{for } (t, x) \in [0, 1] \times [0, 1], \\
 u(t, 0) &= u(t, 1) \quad (\text{Periodic BC}), \\
 u(0, x) &= \sin(2\pi x), \\
 \partial_t u(0, x) &= x(1 - x),
 \end{aligned} \tag{3.5}$$

where ξ is a space-time forcing which we again take as a realisation of white noise. We will compare Algorithm 1 with both models with and without initial conditions. Discretisation of space-time and number of training and test cases is the same as in Section 3.1.1.

Note that, in the general case, the level zero of the full model \mathcal{M}_α^0 for the wave equation should not only include the contribution of the initial condition u_0 but also the contribution of the initial speed $\partial_t u(0, x) = v_0$. This leads to the following definition.

Definition 3.5 Consider an initial condition $u_0 : D \rightarrow \mathbb{R}$, an initial speed $v_0 : D \rightarrow \mathbb{R}$, and a forcing $\xi : [0, T] \times D \rightarrow \mathbb{R}$, as well as $n, m, \ell \geq 1$, $p = 1$, $q \leq 1$. Let $\alpha = (m, \ell, 1, q)$. The model for the wave equation \mathcal{M}_α^n is constructed by taking $\mathcal{J} = \{c, s\}$ with $u^c = I_c[u_0]$, $u^s = I_s[v_0]$ where

$$\begin{cases} (\partial_t^2 - \Delta)I_c[u_0] &= 0 \\ I_c[u_0](0, x) &= u_0(x), \\ \partial_t I_c[u_0](0, x) &= 0. \end{cases} \quad \begin{cases} (\partial_t^2 - \Delta)I_s[v_0] &= 0 \\ I_s[v_0](0, x) &= 0, \\ \partial_t I_s[v_0](0, x) &= v_0(x). \end{cases}$$

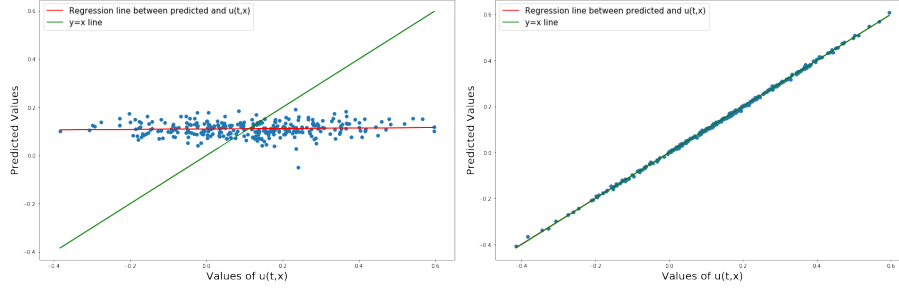
Moreover, for functions $f : [0, T] \times D \rightarrow \mathbb{R}$ the operator $I[f]$ is defined to be the solution to a wave equation

$$(\partial_t^2 - \Delta)I[f] = f,$$

with $I[f](0, x) = \partial_t I[f](0, x) = 0$.

Boundary conditions for the above equation are taken to be the same as boundary conditions for the underlying wave equation (in this case periodic).

For this experiment we choose $n = 4$ and $\alpha = (m, \ell, p, q) = (2, 2, 1, 0)$ and impose the degree to satisfy $\deg \xi = -1.5$, $\deg u_0 = \deg v_0 = -0.5$ and $\beta = 1.5$ in (2.4). We choose only functions of degree ≤ 1.5 which gives 60 functions in \mathcal{M}_α^4 .



(a) Prediction at $(t, x) = (1, 0.5)$ for model with $\mathcal{J} = \emptyset$. Relative l^2 error: 84.1%.
(b) Prediction at $(t, x) = (1, 0.5)$ for model with $\mathcal{J} = \{c, s\}$. Relative l^2 error: 1.8%.

Figure 3: Results of linear regression of solution to (3.5) using functions from models \mathcal{M}_α^4 with $\alpha = (2, 2, 1, 0)$ of degree ≤ 1.5 without and with initial conditions. The x -axis contains values of $u(t, x)$ for realisations of the forcing ξ from the test set and the y -axis contains predictions of the linear regression. Subplots (a), (b) show predictions at space-time point $(t, x) = (1, 0.5)$ for models with $\mathcal{J} = \emptyset$ and $\mathcal{J} = \{c, s\}$ respectively.

Figure 3 shows the importance of using the full model in the case of the wave equation, i.e., the contribution of the initial condition (even fixed and deterministic) can't be ignored.⁸ The model constructed with $\mathcal{J} = \emptyset$ in the case of the wave equation gives absolutely no predictability contrary to the parabolic case (see Remark 3.3) because the wave operator is not dissipative contrary to the heat operator. Average relative l^2 errors corresponding to the height of the model are presented in the Table 2 for 1000 repeated experiments.

Model's Height	1	2	3	4
With initial speed	60.60%	12.86%	2.09%	1.19%
Without initial speed	60.40%	13.45%	5.39%	4.77%

Table 2: Relative l^2 errors for prediction at space-time point $(t, x) = (1, 0.5)$ for different heights of the model. First line includes errors using $\mathcal{J} = \{c, s\}$ the second line includes errors using $\mathcal{J} = \{c\}$ only.

Table 2 further shows the importance of including the contributions of both the initial condition and the initial speed in the model when predicting the wave equation.

⁸This parallels the necessity of including the initial condition in an analogue of the model in [GKO21] where the authors solve a non-linear singular stochastic wave equation in 3 dimensions.

3.3 Burgers' equation

In this subsection, we aim to predict solutions to the following Burgers' equation with no forcing

$$\begin{aligned} (\partial_t - 0.1\partial_x^2)u &= -u\partial_x u \quad (t, x) \in [0, 10] \times [-8, 8] \\ u(t, -8) &= u(t, 8) \quad (\text{Periodic BC}), \\ u_0(x) &= \sum_{k=-10}^{10} \frac{a_k}{1 + |k|^2} \sin(\lambda^{-1}\pi kx) \end{aligned} \quad (3.6)$$

from the knowledge of the initial condition u_0 . This experiment is partly inspired by [MAAA20]. Above, $(a_k)_{k=-10, \dots, 10}$ are sampled as independent and identically distributed (i.i.d.) standard normal random variables and λ is a scaling parameter. We sample 120 such initial conditions with scaling $\lambda = 8, 4, 2$ (40 initial conditions for each scaling), which corresponds to u_0 having respectively one, two and four cycles. We then randomly subdivide these initial conditions into training and test sets of sizes 100 and 20 respectively. We observe 201 time points on $[0, 10]$ ($N = 200$, $\delta = 0.05$) and 512 space points on $D = [-8, 8]$, though the equation itself is solved on a more finer grid (2001 time points and 1024 space points).

The above equation satisfies the time homogeneous flow property necessary for Algorithm 2, which is used in the experiments below. There is no forcing ξ in the equation so $p = \ell = 0$. We construct the models using Definition 3.1. We choose height $n = 3$ and additive width $m = 2$ for the model i.e. $\alpha = (2, 0, 0, 1)$. We assign for the degree $\deg u_0 = -1.5$ and $\beta = 2$ in (2.4) and only functions f_τ with degree $\deg \tau \leq 2.5$ are considered. This gives 20 functions of $\deg \tau \leq 2.5$ instead of the original 91 functions in \mathcal{M}_α^3 . Using this degree cutoff speeds up the fitting of the linear regression by around 20 times in addition to a faster computation of the model.

As the number of training and testing cases (100 and 20) is relatively small, we repeated the above experiment 10 times. The average relative l^2 error over the 20 test cases, when further averaged over the 10 experiments, is 3.04%. The maximum and minimum average relative l^2 error over the 20 test cases in any experiment is 5.3% and 2.1% respectively. Furthermore, in any experiment and test case, the maximum relative l^2 error is 11.4%. Figure 4 shows the heat-maps for the true and predicted solutions drawn from several test cases with varying relative l^2 error.

Algorithm 2 furthermore seems to be stable under adding noise to the observed data. We added a 1% error to the observed data in the following way. Instead of observing the solution u of (3.6), we observe

$$\tilde{u}(t, x) = u(t, x) + \varepsilon(t, x)\sqrt{\|u\|_{\tilde{L}^1}}, \quad (3.7)$$

where $\|u\|_{\tilde{L}^1} = \frac{1}{201 \times 512} \sum_{(t, x)} |u(t, x)|$ (the sum is over the observed grid points of $[0, 10] \times [-8, 8]$) and $\varepsilon(t, x)$ are i.i.d. normal random variables with zero mean and standard deviation 0.01 for each (t, x) for the training data and for $(t, x) = (0, x)$ for the test data. In this case, comparing to the true values from the test set, the average relative l^2 error over the 20 test cases, when further averaged over the 10 experiments, is 7.56% (compared to 3.04% without noise). The maximum and minimum average relative l^2 error over the 20 test cases in any experiment is 9.2% and 5.8% respectively. However, the absolute maximum in any experiment and test case increases quite drastically to 25.3%.

Finally, we ran Algorithm 2 using models in which the viscosity parameter ν in Definition 3.1 is estimated from the data (the true value being $\nu = 0.1$). We estimate ν

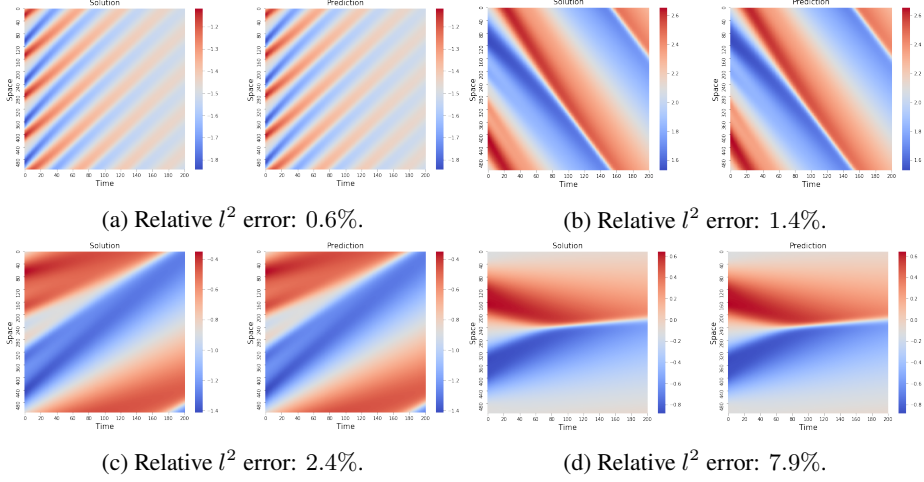


Figure 4: Heat-maps for the solution of (3.6) and predictions for several test cases using Algorithm 2 with functions from the model \mathcal{M}_α^3 with $\alpha = (2, 0, 0, 1)$ of degree ≤ 3.5 .

by simply linearly regressing the discrete time derivative of u against the discrete second derivative in space for $u \in U^{\text{obs}}$. To be more precise, we use ordinary least squares to determine the best $\tilde{\nu}$ that fits

$$(u_{t_1}(x) - u_{t_0}(x))/\delta = \epsilon + \tilde{\nu} \partial_x^2 u_{t_0}(x), \quad u \in U^{\text{obs}}, \quad x \in D,$$

where ∂_x^2 is computed using central finite difference. Such an estimate does not require any knowledge of the non-linearity.

Remark 3.6 Although we do not do this here, one could further use cross-validation to select a find a better estimate for ν from the interval $[\tilde{\nu} - a, \tilde{\nu} + a]$ for some $a > 0$.

The average estimated viscosity over the 10 experiments is 0.091 with the maximum and minimum estimated viscosity over all experiments being 0.113 and 0.084 respectively.

Running the above Algorithm 2 with the estimated viscosity, we find that the results were not much different than those with the correct viscosity $\nu = 0.1$. The average relative l^2 error over the 20 test cases, when further averaged over the 10 experiments, is 3.14% (compared to 3.04% for the true viscosity). The maximum increase of the average relative l^2 error is 0.2% in any experiments.

3.3.1 Comparison with other learning algorithms

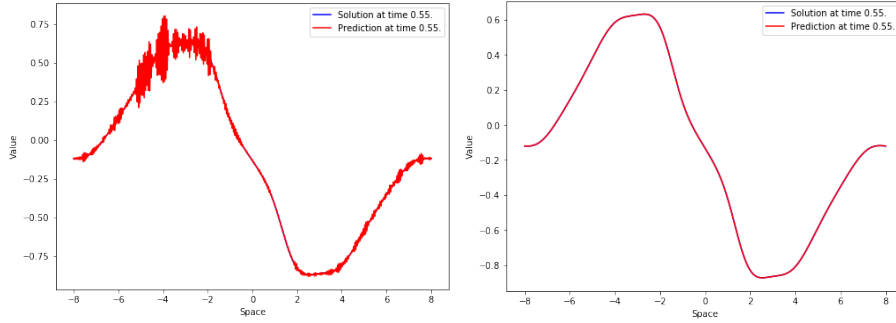
Euler Algorithm. We compare Algorithm 2 in the above experiment to a similar one but where in Step 2 of Algorithm 2, instead of regressing $(u_{t_{j+1}}(x))_{u \in U^{\text{obs}}, j=0, \dots, N-1}$ against $(\mathcal{M}_m^n(j, u))_{u \in U^{\text{obs}}, j=0, \dots, N-1}$, we regress against

$$(\{u_{t_k}(x), \partial_x^2 u_{t_k}(x), u_{t_k}(x) \partial_x u_{t_k}(x)\})_{u \in U^{\text{obs}}, j=0, \dots, N-1}.$$

The motivation for this algorithm is that exactly these terms appear on the right-hand side if we wish to numerically compute $u_{t_{k+1}}(x)$ using finite difference method. A

similar change from the model $\mathcal{M}_\alpha^n(u_{t_k}^{\text{pr}})$ to $\{u_{t_k}^{\text{pr}}(x), \partial_x^2 u_{t_k}^{\text{pr}}(x), u_{t_k}^{\text{pr}}(x)\partial_x u_{t_k}^{\text{pr}}(x)\}$ is made in Step 3 and Step 4. We will call this learning algorithm the Euler Algorithm.

Figure 5 compares 2 predictions at time $t_{11} = 0.55$ for the same test case using the Euler Algorithm and Algorithm 2. Even for prediction at t_1 , for some test cases the Euler Algorithm performs worse than Algorithm 2. For the same test case as on Figure 5, the relative l^2 error for all spatial points between the true values of u_{t_1} and $u_{t_1}^{\text{pr}}$ is 0.2% for the Euler Algorithm compared to 0.1% for Algorithm 2. More importantly, the Euler Algorithm fails to produce good prediction for larger times and already starts to fail for this test case at t_{11} for most of the space points giving 9.7% error compared to 0.07% error from Algorithm 2. At time t_{12} , the Euler Algorithm blows up and gives an error of 244%. Other test cases exhibit a similar blow up for times $t < t_{20}$.



(a) Prediction $u_{t_{11}}^{\text{pr}}$ using the Euler Algorithm. (b) Prediction $u_{t_{11}}^{\text{pr}}$ using Algorithm 2.
Relative l^2 error for all spatial points: 9.7%. Relative l^2 error for all spatial points: 0.07%.

Figure 5: Comparison of predictions using the Euler Algorithm and Algorithm 2. Each subplot contains a graph of $u_{t_{11}}^{\text{pr}} : D \rightarrow \mathbb{R}$.

We believe that the reason why Algorithm 2 seems to be quite stable for all times (even after adding a 1% error from (3.7)) in comparison with the Euler Algorithm is because of the averaging effect of the heat operator I . This means that the error between the corresponding functions in $\mathcal{M}_\alpha^n(u_{t_k}^{\text{pr}})$ and in $\mathcal{M}_\alpha^n(u_{t_k})$ is expected to be smaller than the error between $u_{t_k}^{\text{pr}}$ and u_{t_k} . This means that in Algorithm 2 the error would not accumulate in comparison to the Euler Algorithm.

PDE-FIND. We use a version of PDE-FIND algorithm from [RBPK17] to learn the non-linearity first instead of learning the solution. We use linear regression to find the best coefficients a, b such that

$$\partial_t u(t_k, x) = a \partial_x^2 u(t_k, x) + b u(t_k, x) \partial_x u(t_k, x), \quad u \in U^{\text{obs}}, k = 0, \dots, N-1, x \in D, \quad (3.8)$$

where $\partial_t u(t_k, x) := \frac{u(t_{k+1}, x) - u(t_k, x)}{\delta}$ is a discrete time derivative, ∂_x is discrete space derivative and $x \in D$ are the observed points. Such an approach leads to $(a, b) = (0.12, -0.96)$ (averaged over 10 experiments) instead of the true values $(0.1, -1)$. We then use finite difference method with the estimated (a, b) (estimating these coefficients separately for each experiment) starting from initial conditions from U^{pr} in order to construct the solution on the full domain $[0, 10] \times D$. Note though that in this finite difference we can discretise time on a finer grid. In fact, we take 2001 points on $[0, 10]$ which is the same number of time points that is used to construct solution to (3.6). We

cannot, however, discretise space on a finer grid than 512 points because these are the only points observed for the initial conditions from U^{pr} . Finally, solutions produced by a finite difference method with the estimated (a, b) , 2001 time points on $[0, 10]$ and 512 space points on $[-8, 8]$ give an average relative l^2 error over the 20 test cases, when averaged over the 10 experiments, of 3.45%. Almost every experiment has an average relative l^2 error obtained from Algorithm 2 which is on average 0.65% smaller than the one obtained by PDE-FIND. In only one experiment PDE-FIND outperforms Algorithm 2 with 3.6% compared to 5.3%.

The main advantage of Algorithm 2 over PDE-FIND is that PDE-FIND performs poorly on noisy data like in (3.7). Learning (a, b) from \tilde{u} as in (3.7) instead of u gives a completely wrong estimate for (a, b) , for instance giving $(a, b) = (0.007, -0.078)$ for one of the experiments which is far from the real $(a, b) = (0.1, -1)$. This is because the added noise $\varepsilon(t, x)$ is not differentiable and so the errors in (3.8) become huge. This is not an issue for Algorithm 2 because all the functions in the model \mathcal{M}_α^n are smooth enough to take a spatial derivative thanks to the smoothing properties of the heat operator.

4 Summary and discussion

To summarise, we performed Algorithm 1 to both parabolic and hyperbolic equations with forcing and Algorithm 2 to Burgers equation with varying initial conditions. We did an elementary comparison of our algorithms with other methods. We compared the performance of Algorithm 1 for the parabolic equation with multiplicative forcing against several off-the-shelf methods and found a large advantage in favour of Algorithm 1 (see Remark 3.4). We further compared Algorithm 2 for the Burgers' equation against a version of PDE-FIND [RBPk17] and a naive Euler regression (see Section 3.3.1), and again found an advantage in favour of Algorithm 2. This advantage moreover persisted when noise was added. We believe the success of Algorithm 2 in this experiment is due to the smoothing properties of the heat operator, which provides considerable robustness.

In terms of the hyperparameters, the experiments with Algorithm 1 in Sections 3.1 and 3.2 show that increasing the height of the model gives better predictability. We also found in Section 3.3 that one can effectively estimate the viscosity parameter $\nu > 0$ from the data at the expense of increasing the error from 0.36% to 0.62%. These experiments demonstrate a potential for the use of models as features for learning PDEs. A more systematic comparison of our algorithms with other methods as well as the effect of hyperparameters is left for future work.

We conclude by discussing several other directions in which this work could be extended.

- **Beyond PDEs.** An important next step is to investigate the use of models as features in learning algorithms in contexts beyond PDEs. We believe that natural directions to investigate include analysis of meteorological data [SCW⁺15, CLK⁺18], image and remote sensing recognition [Kriog, ZNZW15], and applications to fluid dynamics [BNK20, LKT16].
- **Further learning algorithms.** It will be important to explore the utility of 'model features' when combined with learning algorithms beyond linear regression (the only tool used in this article), such as with neural networks and random forests. Similarly, it would be important to *kernelise* the model feature vector efficiently. This would allow for use of popular kernel learning methods, such as support

vector machines, and of the maximum mean discrepancy (MMD) of [GBR⁺12] to compare samples drawn from different distributions. An MMD from the kernelised signature map was used in [CO18] to define a metric on the laws of stochastic process indexed by time, and fast signature kernelisation algorithms were introduced in [KO19]; extending these results to models would be of significant interest.

- **Higher dimensions.** In order to apply the ideas in this paper to data in high dimensional spaces, it would be important to improve the computation of models. It took⁹ between 0.2 to 0.5 seconds to compute one model in Sections 3.1 and 3.2, and 582.5 seconds to perform one run of Algorithm 2 in Section 3.3. The computation time in higher spatial dimensions would be significantly longer.

In this direction, there are a number of works aiming to solve high dimensional PDEs with learning algorithms, such as [HJE18, SS18]. Since, with the choice of operator I in our experiments, elements of the models are solutions to special PDEs, it would be interesting to see if these methods could make it feasible to compute the model features in high dimensional spaces.

- **Operator I hyperparameter.** The operator I in the definition of a model is a hyperparameter which needs to be chosen from a very large space (the infinite-dimensional space of linear operators). In our experiments, we mostly used knowledge of the *linear part* of the PDE (heat or wave operators) to choose I . However, if the PDE is completely unknown, or if the output u does not come from a PDE at all, then one would need a systematic way to choose this hyperparameter. The same applies to the other hyperparameters, such as n, m, ℓ, p, q , but these take values in a smaller space for which standard hyperparameter tuning (e.g. cross-validation, or sparse linear regression similar to PDE-FIND [RBPK17]) is feasible. Note that the problem of choosing I does not arise in the context of signatures simply because one hardcodes I as convolution with the Heaviside step function $J(t) = \mathbf{1}_{t>0}$. We could of course likewise hardcode I , e.g., as the inverse of the heat operator (3.2), but if one believes the output u should behave like the solution to a wave equation, this will likely yield poor performance. How to choose I in a general context is therefore an important theoretical and practical question.

Appendix A Motivation

In this appendix we will explain the motivation behind using the model as a feature set for predicting PDEs. For this we will consider a PDE (3.1) and $\mathcal{L} = \partial_t - \Delta$ with non-linearities μ, σ which are independent of $\partial_i u$. The case when μ, σ depend on $\partial_i u$ as well as the case of the wave equation is left to the reader.

Under good enough assumptions on the functions μ, σ, u_0 and the forcing ξ , equation (3.1) admits a local in time mild solution.¹⁰ In particular, Picard's Theorem implies that u is the limit of the following recursive sequence

$$\begin{aligned} u_t^0 &= I_c[u_0]_t \\ u_t^{n+1} &= I_c[u_0]_t + I[\mu(u^n)]_t + I[\sigma(u^n\xi)]_t, \end{aligned} \tag{A.1}$$

⁹On a laptop with 4 Cores (1.4 GHz) and 16 GB memory.

¹⁰In the case that ξ is white noise on $[0, T] \times [0, 1]$, smoothness of the above functions is enough (see [DPZ14]).

where again the operators I and I_c are defined by (3.2). The idea is now to Taylor expand the function μ up to m terms and the function σ up to ℓ terms in the equation for u^{n+1} . Define $u^{0,m,\ell} = I_c[u_0]$ and recursively set

$$u_t^{n+1,m,\ell} = I_c[u_0]_t + \sum_{k=0}^m \frac{\mu^{(k)}(0)}{k!} I[(u^{n,m,\ell})^k]_t + \sum_{k=0}^{\ell} \frac{\sigma^{(k)}(0)}{k!} I[(u^{n,m,\ell})^k \xi]_t. \quad (\text{A.2})$$

We then see, heuristically, that since Taylor's expansion implies $u_t^{n,m,\ell} \rightarrow u_t^n$ as $m, \ell \rightarrow \infty$ and since by Picard iteration $u_t^n \rightarrow u_t$ as $n \rightarrow \infty$ then $u_t^{n,m,\ell}$ could be a good candidate for approximating u_t .

It is not difficult to see from (A.2) that $u^{n,m,\ell}(t, x)$ is a linear combination of $\{f_\tau(t, x)\}_{\tau \in \mathcal{S}_\alpha^n}$ for $\alpha = (m, \ell + 1, 1, 0)$. This concludes our heuristic motivation for using the model \mathcal{M}_α^n as a set of features for linear regression of solution to (3.1).

Remark A.1 If it is known that the equation (3.1) is additive, i.e. that σ is a constant, then the above heuristic suggests that one should consider \mathcal{M}_α^n with $\ell = p = 1$. More generally, if it is known that both μ and σ are polynomials, then the heuristic suggests that taking m and $\ell - 1$ greater than the respective degrees of μ and σ would likely not improve the accuracy of the above algorithm. These remarks follow from the fact that polynomials agree with their Taylor expansion (for high enough order of expansion).

References

- [AGG⁺18] I. P. ARRIBAS, G. M. GOODWIN, J. R. GEDDES, T. LYONS, and K. E. A. SAUNDERS. A signature-based machine learning model for distinguishing bipolar disorder and borderline personality disorder. *Transl. Psychiatry* **8**, no. 274(2018). doi: 10.1038/s41398-018-0334-0.
- [BGLY16] H. BOEDIHARDJO, X. GENG, T. LYONS, and D. YANG. The signature of a rough path: Uniqueness. *Advances in Mathematics* **293**, (2016), 720–737. doi:https://doi.org/10.1016/j.aim.2016.02.011.
- [BHZ19] Y. BRUNED, M. HAIRER, and L. ZAMBOTTI. Algebraic renormalisation of regularity structures. *Invent. Math.* **215**, no. 3, (2019), 1039–1156. arXiv:1610.08468. doi:10.1007/s00222-018-0841-x.
- [BNK20] S. L. BRUNTON, B. R. NOACK, and P. KOUMOUTSAKOS. Machine learning for fluid mechanics. *Annual Review of Fluid Mechanics* **52**, no. 1, (2020), 477–508. arXiv: https://doi.org/10.1146/annurev-fluid-010719-060214. doi:10.1146/annurev-fluid-010719-060214.
- [BSHHB19] Y. BAR-SINAI, S. HOYER, J. HICKEY, and M. P. BRENNER. Learning data-driven discretizations for partial differential equations. *Proc. Natl. Acad. Sci. USA* **116**, no. 31, (2019), 15344–15349. doi:10.1073/pnas.1814058116.
- [Che58] K.-T. CHEN. Integration of paths—a faithful representation of paths by non-commutative formal power series. *Trans. Amer. Math. Soc.* **89**, (1958), 395–407. doi:10.2307/1993193.
- [CK16] I. CHEVYREV and A. KORMILITZIN. A primer on the signature method in machine learning, 2016. arXiv:1603.03788.
- [CL16] I. CHEVYREV and T. LYONS. Characteristic functions of measures on geometric rough paths. *Ann. Probab.* **44**, no. 6, (2016), 4049–4082. doi:10.1214/15-AOP1068.

- [CLK⁺18] G. CHEN, S. LI, L. D. KNIBBS, N. HAMM, W. CAO, T. LI, J. GUO, H. REN, M. J. ABRAMSON, and Y. GUO. A machine learning method to estimate pm2.5 concentrations across china with remote sensing, meteorological and land use information. *Science of The Total Environment* **636**, (2018), 52–60. doi:<https://doi.org/10.1016/j.scitotenv.2018.04.251>.
- [CNO20] I. CHEVYREV, V. NANDA, and H. OBERHAUSER. Persistence paths and signature features in topological data analysis. *IEEE Transactions on Pattern Analysis and Machine Intelligence* **42**, no. 1, (2020), 192–202. doi:[10.1109/TPAMI.2018.2885516](https://doi.org/10.1109/TPAMI.2018.2885516).
- [CO18] I. CHEVYREV and H. OBERHAUSER. Signature moments to characterize laws of stochastic processes. *arXiv e-prints* arXiv:1810.10971. arXiv:1810.10971.
- [DPZ14] G. DA PRATO and J. ZABCZYK. *Stochastic equations in infinite dimensions*, vol. 152 of *Encyclopedia of Mathematics and its Applications*. Cambridge University Press, Cambridge, second ed., 2014, xviii+493. doi:[10.1017/CBO9781107295513](https://doi.org/10.1017/CBO9781107295513).
- [GBR⁺12] A. GRETTON, K. M. BORGWARDT, M. J. RASCH, B. SCHÖLKOPF, and A. SMOLA. A kernel two-sample test. *J. Mach. Learn. Res.* **13**, (2012), 723–773.
- [GKO21] M. GUBINELLI, H. KOCH, and T. OH. Paracontrolled approach to the three-dimensional stochastic nonlinear wave equation with quadratic nonlinearity, 2021. arXiv:1811.07808. To appear in J. Eur. Math. Soc.
- [Gra13] B. GRAHAM. Sparse arrays of signatures for online character recognition, 2013. arXiv:1308.0371.
- [Hai14] M. HAIRER. A theory of regularity structures. *Invent. Math.* **198**, no. 2, (2014), 269–504. arXiv:1303.5113. doi:[10.1007/s00222-014-0505-4](https://doi.org/10.1007/s00222-014-0505-4).
- [HJE18] J. HAN, A. JENTZEN, and W. E. Solving high-dimensional partial differential equations using deep learning. *Proc. Natl. Acad. Sci. USA* **115**, no. 34, (2018), 8505–8510. doi:[10.1073/pnas.1718942115](https://doi.org/10.1073/pnas.1718942115).
- [HJLC⁺84] F. E. HARRELL JR, K. L. LEE, R. M. CALIFF, D. B. PRYOR, and R. A. ROSATI. Regression modelling strategies for improved prognostic prediction. *Statistics in medicine* **3**, no. 2, (1984), 143–152. doi:[10.1002/sim.4780030207](https://doi.org/10.1002/sim.4780030207).
- [HL10] B. HAMBLY and T. LYONS. Uniqueness for the signature of a path of bounded variation and the reduced path group. *Ann. of Math. (2)* **171**, no. 1, (2010), 109–167. doi:[10.4007/annals.2010.171.109](https://doi.org/10.4007/annals.2010.171.109).
- [KBPA⁺19] P. KIDGER, P. BONNIER, I. PEREZ ARRIBAS, C. SALVI, and T. LYONS. Deep signature transforms. In *Advances in Neural Information Processing Systems* 32, 3105–3115. Curran Associates, Inc., 2019.
- [KLA20] J. KALSI, T. LYONS, and I. P. ARRIBAS. Optimal Execution with Rough Path Signatures. *SIAM J. Financial Math.* **11**, no. 2, (2020), 470–493. doi:[10.1137/19M1259778](https://doi.org/10.1137/19M1259778).
- [KO19] F. J. KIRALY and H. OBERHAUSER. Kernels for sequentially ordered data. *Journal of Machine Learning Research* **20**, no. 31, (2019), 1–45.
- [Kri09] A. KRIZHEVSKY. Learning multiple layers of features from tiny images. Technical report, Department of Computer Science, University of Toronto, 2009.
- [LKT16] J. LING, A. KURZAWSKI, and J. TEMPLETON. Reynolds averaged turbulence modelling using deep neural networks with embedded invariance. *Journal of Fluid Mechanics* **807**, (2016), 155–166. doi:[10.1017/jfm.2016.615](https://doi.org/10.1017/jfm.2016.615).
- [LNA19] T. LYONS, S. NEJAD, and I. P. ARRIBAS. Numerical Method for Model-free Pricing of Exotic Derivatives in Discrete Time Using Rough Path Signatures. *Appl.*

- Math. Finance* **26**, no. 6, (2019), 583–597. doi:10.1080/1350486X.2020.1726784.
- [LPS14] G. J. LORD, C. E. POWELL, and T. SHARDLOW. *An introduction to computational stochastic PDEs*. Cambridge Texts in Applied Mathematics. Cambridge University Press, New York, 2014, xii+503. doi:10.1017/CBO9781139017329.
- [Ly098] T. J. LYONS. Differential equations driven by rough signals. *Rev. Mat. Iberoamericana* **14**, no. 2, (1998), 215–310. doi:10.4171/RMI/240.
- [LZJ17] C. LI, X. ZHANG, and L. JIN. LPSNet: A novel log path signature feature based hand gesture recognition framework. In *2017 IEEE International Conference on Computer Vision Workshops (ICCVW)*, 631–639. 2017.
- [MAAA20] S. MALIK, U. ANWAR, A. AHMED, and A. AGHASI. Learning to solve differential equations across initial conditions. In *ICLR 2020 Workshop on Integration of Deep Neural Models and Differential Equations*. 2020.
- [MKN⁺19] J. MORRILL, A. KORMILITZIN, A. NEVADO-HOLGADO, S. SWAMINATHAN, S. HOWISON, and T. LYONS. The signature-based model for early detection of sepsis from electronic health records in the intensive care unit. In *2019 Computing in Cardiology (CinC)*, Page 1–Page 4. 2019.
- [MQdH18] M. MAGILL, F. QURESHI, and H. DE HAAN. Neural networks trained to solve differential equations learn general representations. In S. BENGIO, H. WALLACH, H. LAROCHELLE, K. GRAUMAN, N. CESA-BIANCHI, and R. GARNETT, eds., *Advances in Neural Information Processing Systems*, vol. 31. Curran Associates, Inc., 2018.
- [RBPk17] S. H. RUDY, S. L. BRUNTON, J. L. PROCTOR, and J. N. KUTZ. Data-driven discovery of partial differential equations. *Science Advances* **3**, no. 4, (2017), e1602614. doi:10.1126/sciadv.1602614.
- [RMB⁺09] C. W. ROWLEY, I. MEZIĆ, S. BAGHERI, P. SCHLATTER, and D. S. HENNINGSON. Spectral analysis of nonlinear flows. *J. Fluid Mech.* **641**, (2009), 115–127. doi:10.1017/S0022112009992059.
- [RPk19] M. RAISSI, P. PERDIKARIS, and G. E. KARNIADAKIS. Physics-informed neural networks: a deep learning framework for solving forward and inverse problems involving nonlinear partial differential equations. *J. Comput. Phys.* **378**, (2019), 686–707. doi:10.1016/j.jcp.2018.10.045.
- [Sch10] P. J. SCHMID. Dynamic mode decomposition of numerical and experimental data. *J. Fluid Mech.* **656**, (2010), 5–28. doi:10.1017/S0022112010001217.
- [SCW⁺15] X. SHI, Z. CHEN, H. WANG, D.-Y. YEUNG, W.-K. WONG, and W.-C. WOO. Convolutional lstm network: A machine learning approach for precipitation nowcasting. In *Proceedings of the 28th International Conference on Neural Information Processing Systems - Volume 1, NIPS’15*, 802–810. MIT Press, Cambridge, MA, USA, 2015.
- [SS18] J. SIRIGNANO and K. SPILIOPOULOS. DGM: a deep learning algorithm for solving partial differential equations. *J. Comput. Phys.* **375**, (2018), 1339–1364. doi:10.1016/j.jcp.2018.08.029.
- [XSJ⁺18] Z. XIE, Z. SUN, L. JIN, H. NI, and T. LYONS. Learning spatial-semantic context with fully convolutional recurrent network for online handwritten chinese text recognition. *IEEE Transactions on Pattern Analysis and Machine Intelligence* **40**, no. 8, (2018), 1903–1917. doi:10.1109/TPAMI.2017.2732978.
- [ZNZW15] Q. ZOU, L. NI, T. ZHANG, and Q. WANG. Deep learning based feature selection for remote sensing scene classification. *IEEE Geoscience and Remote Sensing Letters* **12**, no. 11, (2015), 2321–2325.